Extending the Operational Land Imager/Landsat 8 for inland water research: retrieval of an orange band from Pan and MS bands

Alexandre Castagna[*1], Stefan Simis[2], Heidi Dierssen[3], Quinten Vanhellemont[4], Koen Sabbe[1], and Wim Vyverman[1]

[1]*Protistology and Aquatic Ecology, Gent University, Krijgslaan 281, Gent 9000, BE*
[2]*Plymouth Marine Laboratory, Prospect Place, The Hoe, PL1 3DH Plymouth, UK*
[3]*Department of Marine Science, University of Connecticut, Groton, CT 06340, USA*
[4]*Ecosystems Data Processing and Modelling, Royal Belgian Institute of Natural Sciences, Brussels 1000, BE*

1 Introduction

The typical spatial resolution of 250 m to 1 km offered by dedicated orbital Ocean Colour (OC) sensors is often inadequate to fully resolve processes occurring in coastal, transitional and inland waters (CEOS, 2018; Muller-Karger et al., 2018). For inland waters, underrepresentation is substantial, with most systems unresolved at those moderate resolutions due to their size and shape (Andreadis et al., 2013; CEOS, 2018; Verpoorter et al., 2014). The requirement of higher spatial resolution has led to the development of water applications for sensors originally designed for terrestrial remote sensing (*e.g.*, Franz et al., 2015; Trinh et al., 2017; Vanhellemont and Ruddick, 2014), the most relevant of which are the Landsat and Sentinel-2 series. The sensors in those platforms offer global coverage at high spatial resolution (10 to 60 m) and feature near infrared (NIR) and shortwave infrared (SWIR) bands appropriate for atmospheric correction over turbid waters (Franz et al., 2015; Vanhellemont and Ruddick, 2015). However, they feature fewer and broader multispectral (MS) bands in the visible range than the standard OC sensors, limiting the the type of algorithms that can be applied, and hence the water quality parameters that can be retrieved.

The Operational Land Imager (OLI) on Landsat 8 resolves four visible bands covering the ultra-blue (435-451 nm), blue (452-512 nm), green (533-590 nm) and red (636-673 nm) and has found successful application for remote sensing of water quality (*e.g.*, Lee et al., 2016; Ogashawara et al., 2016; Olmanson et al., 2016). The waveband configuration, however, does not allow retrieving direct information related to phycocyanin (PC) abundance, a diagnostic pigment for cyanobacteria presence, a major concern for in inland waters. Cyanobacteria blooms are an increasingly frequent phenomenon, and can produce noxious

---

[*]alexandre.castagna@ugent.be

and toxic compounds that cause health risks to wildlife and humans, as well as taste and odor problems in drinking water (Stumpf et al., 2012; Visser et al., 2016). The presence of an orange band (~620 nm) covering the PC absorption peak has allowed specific algorithms to be developed and applied to the OC sensor Medium Resolution Imaging Spectrometer (MERIS) (Kutser et al., 2006; Matthews et al., 2012; Simis et al., 2005, 2007) and its follow-on, the Ocean and Land Colour Instrument (OLCI). At present, high spatial resolution orange bands are only available on commercial sensors, notably the imagers on WorldView-2 and 3.

In addition to the visible bands, OLI also features a high spatial resolution (15 m) panchromatic (Pan) band spanning green to red wavelengths (503-676 nm). Pan bands are commonly used in remote sensing applications to resolve features at higher spatial resolution than provided in the MS channels, made possible due to the wider spectral integration. The high spatial information of the Pan band is merged with the spectral information of the MS bands in a process referred to as pansharpening, producing a final image with the highest possible spatial resolution (*e.g.* Nikolakopoulos, 2008). Here, we propose to use the Pan band not to enhance spatial information, but to enhance spectral information. The objective is to extract a virtual orange (590-635 nm) band, or *contra-*band, from the Pan band, using the green and red MS bands. To our knowledge, this is the first such application of the Pan band to derive a new spectral channel. The addition of the orange band has the potential to greatly expand water quality research and monitoring using the OLI sensor (CEOS, 2018). Routine retrieval of this band through implementation in atmospheric correction software will provide an unprecedented open-access global dataset of orange reflectance at high spatial resolution.

2 Approach

The integration of spectral radiance ($L(\lambda)$) into discrete wavebands performed by the sensor assembly is described by the spectral response function (SRF). Mathematically, this integration can be decomposed into a sum of the integrals of its component spectral regions:

$$\int_{\lambda_{min}}^{\lambda_{max}} L(\lambda)SRF(\lambda)d\lambda = \sum_{i=1}^{n} \int_{\lambda_{min}\in i}^{\lambda_{max}\in i} L(\lambda)SRF(\lambda)d\lambda \ , \tag{1}$$

as long as the regions i do not overlap and their collection fully cover the SRF space. For the OLI sensor (Fig. 1A), the regions in the Pan band delimited by the boundaries of the Full Width at Half Maximum (FWHM) of the green and red MS bands are shown in Fig. 1B. Due to the equivalent center, FWHM and similar spectral profile, the radiance signal resulting from the scaled regions 2 and 4 will be approximately equal to that observed by the green and red MS bands, respectively. Therefore, the use of green and red MS radiances to predict the contributions of regions 2 and 4 to the Pan radiance is straightforward, requiring only a scaling to account for the fractional contribution of those regions to the overall Pan signal. And by difference of those regions with the Pan band, it is then possible to retrieve an independent composite band, *i.e.* the combination of region 1, with FWHM covering the spectrum from 503 to 533 nm (turquoise), and

region 3, from 590 to 635 nm (orange). This composite band, however, mixes spectral information of different components and optical processes. For instance, region 1 will receive a much higher influence from detrital and dissolved organic absorption than region 3. It is necessary then to isolate the information of those remaining regions.

The superposition of the defined regions with the spectral mass specific *in vivo* absorption coefficient of different pigments, $^*a_{pig}$ ($m^2\,mg^{-1}$), is presented in Fig. 1B. It shows that region 1 is in the minimum pigment absorption zone, dominated by carotenoids, while region 3 includes the PC peak, the smaller red Chlorophyll *a* absorption peak and Chlorophyll *c*. For inland waters, where cyanobacteria blooms are a significant environmental threat, it can be expected that region 3 will present a wider range of variation from the other regions. Region 1 is not strongly affected by pigments but will be correlated with signals from adjacent bands due to particle scattering in addition to carotenoids, inorganic and organic absorption (detrital and dissolved). If this correlation is sufficiently high, the turquoise region can be estimated by a MS band alone within acceptable errors, allowing for the retrieval of an independent orange band. The green MS band is the closest to region 1 inside the Pan relative SRF (RSRF) and can be used for that estimation through regression. A similar approach can be applied for the red MS band and region 4 of the Pan to compensate for the small dissimilarities at the NIR end. The updated scheme result in the isolation of the orange signal. However, it is more advantageous to perform a single multiple linear regression involving the green and red MS bands and the Pan band than the separate regressions of the two MS bands. From an bio-optical point of view, this approach takes advantage of the covariance between adjacent bands, caused by broad absorption patterns of the optically active components. Signal from the chlorophylls (Chl) is shared between the red and orange band, as is PC between the orange and the green (*c.f.* Simis and Kauko (2012); Fig. 1B). The single regression equation incorporating the relevant bands is described by:

$$\rho_w^{orange} = \beta_{Pan}\rho_w^{Pan} + \beta_{green}\rho_w^{green} + \beta_{red}\rho_w^{red} \tag{2}$$

where β coefficients carry information on the scaling and proportionality of the original MS bands and the respective unscaled regions of the Pan band. In Eq. 2, ρ_w is the water-leaving reflectance (unitless).

3 Analysis

A diverse *in situ* dataset of 369 ρ_w collected over Dutch and Belgian lakes was used for calibration and validation of Eq. 2. The Dutch dataset was collected over lakes Loosdrecht and IJsselmeer between 2003 and 2005 and are fully described in Simis et al. (2005, 2007). The Belgian dataset was collected over the lakes Donkmeer and Hazewinkel, and the Spuikom lagoon in 2017. With the exception of the Hazewinkel, all lakes are shallow (1.5 to 4.4 m), experiencing wind induced resuspension of bottom sediments and all except the Spuikom, a brackish water system, experience cyanobacteria blooms. Secchi disk depths range from 6 to 0.2 m, with Chl *a* varying between 1.6 and 600 mg m^{-3}.

For both datasets, reflectances were calculated from radiances measured with portable, hand held spectrometers. For the Dutch campaigns a PR-650 (Photo Research, Inc.,

Chatsworth, CA, USA) with 1° Field of View (FOV) foreoptics was used. The instrument has 8 nm FWHM with a spectral sampling of 4 nm, covering the range from 380 to 780 nm. For the Belgian campaigns, a HandHeld FieldSpec (Analytical Spectral Devices, Inc., Boulder, CO, USA) with 7.5° FOV foreoptics was used. The instrument has 3.6 nm FWHM and spectral sampling of 1.6 nm, covering the range from 325 to 1075 nm. For both datasets, spectral surface downwelling plane irradiance ($E_d(\lambda, 0^+)$) was estimated from near-coincident measurements of the surface radiance of a Spectralon™ target, held parallel to the surface. In Dutch campaigns, the classical above water approach was employed, where radiance from the water target was measured at 42° of nadir, with a relative azimuth of 90° to the Sun. Correction for the sky glint component was performed with a fixed surface reflectance factor of 0.029 applied to sky radiance measurement performed at 42° of zenith and equal relative azimuth (Simis et al., 2005, 2007). For Belgian campaigns, reflectances were calculated with a variant of the sky-blocked approach (SBA) presented by Lee et al. (2013), with shadowing correction calculated with a Monte Carlo radiative transfer code (Castagna et al., in prep.).

While pigment data was acquired for all lakes, in this study only the pigment information for the IJsselmeer will be used. It is the only lake in our dataset for which analysis combined High-Performance Liquid Chromatography (HPLC) for organically soluble pigments with spectrophotometric analysis of PC, as described in (Simis et al., 2005, 2007).

Regression analysis of Eq. 2 is performed with Ordinary Least Squares (OLS) based on a random subsample of half the *in situ* dataset, and validated with the complementary set. To retrieve a robust set of coefficients, and describe their uncertainties, the procedure is repeated 10,000 times over unique random subsets of the dataset. Error propagation analysis is performed with the addition of random noise expected at typical top of atmosphere (TOA) radiances and typical clear skies $E_d(\lambda, 0^+)$. Random deviates from error distributions of each band are generated and performance evaluated 10,000 times. The presence of independent information, that is, information not already present in the adjacent MS bands was evaluated by comparing the PC to Chl a ratio with the residuals of the proposed model and with those of a reduced model that do not include a Pan band. The objective is to show in which conditions, if any, the retrieval of an orange band adds new information to the OLI MS dataset.

The generality of the coefficients fitted to the *in situ* datasets were evaluated against the average standardized spectra of the Optical Water Types (OWT) representative of inland waters in the LIMNADES dataset (Spyrakos et al., 2017). This analysis was done to investigate the generality of the approach across OWT, and whether type-specific coefficient are required. All evaluations presented here are for the average coefficients from the resampling procedure. Statistics of performance are the coefficient of determination (R^2), the Root Mean Squared Error (RMSE), the Mean Absolute Percentage Error (MAPE) and the bias, calculated as the mean percentage error. All analysis were performed in R version 3.3.3 (R Core Team, 2017).

4 Results and discussion

The estimation of region 1+2 (Fig 1B) from the green MS band was analysed using the *in situ* data set. The RMSE of the combined region was 6.51×10^{-4}, or about 1% of the minimum value in the dataset, resulting in a MAPE of 2%. The estimation of region 4 from the red MS band resulted in a MAPE of 0.36%, and hence the error in the orange *contra*-band retrieval is dominated by the retrieval of region 1+2. The estimation of the orange band using Eq. 2 leaded to a MAPE of 3.15% and a bias of -0.76% (Fig. 2A). The average coefficients for Eq. 2, with their standard deviations (SD) reported in parenthesis, were:

$$\rho_w^{orange} = 2.4120(\pm 0.1143)\rho_w^{Pan} - 0.9738(\pm 0.0503)\rho_w^{green} - 0.2999(\pm 0.0667)\rho_w^{red} \quad (3)$$

The performance results are presented for the complete dataset, using the average coefficients from the 10,000 random replicates. However, algorithm performance was robust for the independent validation across the replicates. The average and SD of RMSE, MAPE and bias for an orange band retrieval were 9.562×10^{-4} ($\pm 6.342 \times 10^{-5}$), 3.19% ($\pm 0.16\%$), -0.76% ($\pm 0.42\%$), respectively. This indicates that the algorithm is not particularly dependent on the subset of data used for its calibration and validation. Those performances are encouraging, but related to retrieval when uncertainty is negligible in the input data.

Even for accurately calibrated sensors, uncertainty is expected to arise from random noise. Considering typical values of $E_d(\lambda, 0^+)$ for a sun zenith angle of $40°$, the signal to noise ratio (SNR) of the OLI sensor at typical TOA radiance results in an average absolute noise of 2.45×10^{-4}, 2.68×10^{-4} and 3.950×10^{-4} in equivalent ρ_w for green, red and Pan bands, respectively. Using the folded normal distribution as a model of the absolute noise, the generating normal error distributions were calculated to have a mean of zero and SD equal to the average absolute noise scaled by $\sqrt{\pi/2}$. The final performance in the presence of typical noise as expressed by the RMSE, MAPE and bias were 1.549×10^{-3} ($\pm 5.319 \times 10^{-5}$), 5.99% ($\pm 0.26\%$), -0.77% ($\pm 0.39\%$), respectively (Fig. 2B). The average uncertainty of $\sim 6\%$ is typically expected from the OLI band specifications, but may depend on the performance of the atmospheric correction.

When evaluated against the 13 average spectra of the inland OWT (Fig. 3A), the orange band retrieval is within the algorithm uncertainty for 11 types (Fig. 3B). Larger errors are found for two relativelly blue-enhanced OWT (I-3 and I-13), representative of waters with low Chl a (< 1.6 mg m^{-3}) concentration (Spyrakos et al., 2017). A cluster classification with the OWT reveals that the OWT I-1, I-3, I-10 and I-13 are not represented in our *in situ* dataset. Further study is necessary to propose a set of coefficients for low chlorophyll waters and a future version of the algorithm should flag those spectral shapes. We highlight, however, the robust performance of the algorithm for the majority of the OWT. In particular, it is applicable to spectral shapes with moderate to high phytoplankton biomass, conditions in which the ability to detect cyanobacteria blooms is relevant. A better matching of the short wavelength end of the Pan and green bands would improve the orange band retrieval to a MAPE of $< 1\%$ and independent of spectral shape.

Finally, the arguments that favor the application of a single multiple regression equation

5

also raise the question if the orange band has any additional information not already contained in the adjacent green and red MS bands. Answering this question is important, but not straightforward. It is expected that for most spectra with pigment absorption dominated by Chl a and/or Chl c, the information content in the orange region will be completely contained in the red MS band. However, the increasing presence of Chl b, PC and/or PE are expected to result in an increase of the amount of independent information contained in the orange region relative to the green and red (*c.f.* Fig. 1B). Our approach is to contrast the orange estimation with and without the use of the Pan band. The MAPE for a regression with only the green and red MS bands is two times higher than the full model without added noise, $\sim 6\%$ (Fig. 4A; *c.f.* Fig. 2A). But more relevant is that the residuals from the reduced model have a higher linear correlation with the PC to Chl a ratio (Fig. 4B). Especially at PC to Chl a ratios > 0.5, where the absorption in the orange band is no longer dominated by Chl a, the proposed full model performs significantly better. PC to Chl a ratios > 0.5 are typically needed for accurate PC retrieval (Li and Song, 2017).

5 Conclusions

In this study we proposed and validated a method for retrieval of water-leaving reflectance in the orange range (590 to 635 nm) from the Pan band of OLI/Landsat 8, with an average uncertainty of 6% in the presence of typical noise. We demonstrated the generality of the algorithm for inland waters with Chl a higher than 1.6 mg m^{-3} and showed how the orange band can provide independent information in the presence of PC. The method is made available in the free and open source atmospheric correction code ACOLITE (https://odnature.naturalsciences.be/remsem/software-and-data/acolite).

The orange *contra*-band covers the absorption of PC, a diagnostic pigment of cyanobacteria in inland waters. This specific information can be used for detecting cyanobacteria presence beyond regional correlations. The high spatial resolution, global coverage and free data policy of OLI allow for global, continous application since 2013.

We note the generality of the approach of retrieval of an additional band for multispectral sensors. The spectral enhancement resulting in a *contra*-band can be applied to any sensor with overlapping bands. It can be applied to legacy and current sensors and should be used as guidance for design of broad bands overlaping with MS bands in future sensors, maximizing the spectral information derived from a single sensor operating at multiple spatial and spectral resolutions. To reduce the uncertainty associated with retrieval over variable spectral shapes, the shorter range band(s) should be completly included in the larger range band, matching one extreme of their FWHM.

Future work will progress for application in coastal waters, to adress the effects of carotenoids and Chl c, and to implement automatic detection of spectral shapes for appropriate coefficient selection.

References

Andreadis, K. M., Schumann, G. J., and Pavelsky, T. A simple global river bankfull width and depth database. *Water Resources Research*, 49(10):7164–7168, 2013. doi: 10.1002/wrcr.20440.

CEOS. Feasibility Study for an Aquatic Ecosystem Earth Observing System. Technical report, Committee on Earth Observation Satellites (CEOS), 2018.

Franz, B. A., Bailey, S. W., Kuring, N., and Werdell, P. J. Ocean color measurements with the Operational Land Imager on Landsat-8 : implementation and evaluation in SeaDAS. *Journal of Applied Remote Sensing*, 9(1):096070, 2015. doi: 10.1117/1.JRS.9.096070.

Hoepffner, N. and Sathyendranath, S. Determination of the major groups of phytoplankton pigments from the absorption spectra of total particulate matter. *Journal of Geophysical Research*, 98(C12):22789, 1993. doi: 10.1029/93JC01273.

Kutser, T., Metsamaa, L., Strömbeck, N., and Vahtmäe, E. Monitoring cyanobacterial blooms by satellite remote sensing. *Estuarine, Coastal and Shelf Science*, 67(1-2): 303–312, 2006. doi: 10.1016/j.ecss.2005.11.024.

Lee, Z., Pahlevan, N., Ahn, Y.-H., Greb, S., and O'Donnell, D. Robust approach to directly measuring water-leaving radiance in the field. *Applied Optics*, 52(8):1693, 2013. doi: 10.1364/AO.52.001693.

Lee, Z., Shang, S., Qi, L., Yan, J., and Lin, G. A semi-analytical scheme to estimate Secchi-disk depth from Landsat-8 measurements. *Remote Sensing of Environment*, 177: 101–106, 2016. doi: 10.1016/j.rse.2016.02.033.

Li, L. and Song, K. Bio-optical Modeling of Phycocyanin. In Mishra, D. R., Ogashawara, I., and Gitelson, A. A., editors, *Bio-optical Modeling and Remote Sensing of Inland Waters*, chapter 8, pages 233–262. Elsevier, Chippenham, UK, 2017. doi: 10.1016/B978-0-12-804644-9.00008-2.

Matthews, M. W., Bernard, S., and Robertson, L. An algorithm for detecting trophic status (chlorophyll-a), cyanobacterial-dominance, surface scums and floating vegetation in inland and coastal waters. *Remote Sensing of Environment*, 124:637–652, 2012. doi: 10.1016/j.rse.2012.05.032.

Muller-Karger, F. E., Hestir, E., Ade, C., Turpie, K., Roberts, D. A., Siegel, D., Miller, R. J., Humm, D., Izenberg, N., Keller, M., Morgan, F., Frouin, R., Dekker, A. G., Gardner, R., Goodman, J., Schaeffer, B., Franz, B. A., Pahlevan, N., Mannino, A. G., Concha, J. A., Ackleson, S. G., Cavanaugh, K. C., Romanou, A., Tzortziou, M., Boss, E. S., Pavlick, R., Freeman, A., Rousseaux, C. S., Dunne, J., Long, M. C., Klein, E., McKinley, G. A., Goes, J., Letelier, R., Kavanaugh, M., Roffer, M., Bracher, A., Arrigo, K. R., Dierssen, H., Zhang, X., Davis, F. W., Best, B., Guralnick, R., Moisan, J., Sosik, H. M., Kudela, R., Mouw, C. B., Barnard, A. H., Palacios, S., Roesler, C., Drakou, E. G., Appeltans, W., and Jetz, W. Satellite sensor requirements for monitoring essential biodiversity variables of coastal ecosystems. *Ecological Applications*, 28 (3):749–760, 2018. doi: 10.1002/eap.1682.

Nikolakopoulos, K. G. Comparison of Nine Fusion Techniques for Very High Resolution Data. *Photogrammetric Engineering and Remote Sensing*, 74(5):647–659, 2008.

Ogashawara, I., Li, L., and Moreno-Madriñán, M. J. Slope algorithm to map algal blooms in inland waters for Landsat 8/Operational Land Imager images. *Journal of Applied Remote Sensing*, 11(1):012005, 2016. doi: 10.1117/1.JRS.11.012005.

Olmanson, L. G., Brezonik, P. L., Finlay, J. C., and Bauer, M. E. Comparison of Landsat 8 and Landsat 7 for regional measurements of CDOM and water clarity in lakes. *Remote Sensing of Environment*, 185:119–128, 2016. doi: 10.1016/j.rse.2016.01.007.

R Core Team. *R: A Language and Environment for Statistical Computing*. R Foundation for Statistical Computing, Vienna, Austria, 2017. URL https://www.R-project.org/.

Simis, S. G. H. and Kauko, H. M. In vivo mass-specific absorption spectra of phycobilipigments through selective bleaching. *Limnology and Oceanography: Methods*, 10 (4):214–226, 2012. doi: 10.4319/lom.2012.10.214.

Simis, S. G. H., Peters, S. W. M., and Gons, H. J. Remote sensing of the cyanobacterial pigment phycocyanin in turbid inland water. *Limnology and Oceanography*, 50(1): 237–245, 2005. doi: 10.4319/lo.2005.50.1.0237.

Simis, S. G. H., Ruiz-Verdú, A., Domínguez-Gómez, J. A., Peña-Martinez, R., Peters, S. W., and Gons, H. J. Influence of phytoplankton pigment composition on remote sensing of cyanobacterial biomass. *Remote Sensing of Environment*, 106(4):414–427, 2007. doi: 10.1016/j.rse.2006.09.008.

Spyrakos, E., O'Donnell, R., Hunter, P. D., Miller, C., Scott, M., Simis, S. G. H., Neil, C., Barbosa, C. C. F., Binding, C. E., Bradt, S., Bresciani, M., Dall'Olmo, G., Giardino, C., Gitelson, A. A., Kutser, T., Li, L., Matsushita, B., Martinez-Vicente, V., Matthews, M. W., Ogashawara, I., Ruiz-Verdú, A., Schalles, J. F., Tebbs, E., Zhang, Y., and Tyler, A. N. Optical types of inland and coastal waters. *Limnology and Oceanography*, 2(63):846–870, 2017. doi: 10.1002/lno.10674.

Stumpf, R. P., Wynne, T. T., Baker, D. B., and Fahnenstiel, G. L. Interannual Variability of Cyanobacterial Blooms in Lake Erie. *PloS one*, 7(8):e42444, 2012. doi: 10.1371/journal.pone.0042444.

Trinh, R. C., Fichot, C. G., Gierach, M. M., Holt, B., Malakar, N. K., Hulley, G., and Smith, J. Application of Landsat 8 for Monitoring Impacts of Wastewater Discharge on Coastal Water Quality. *Frontiers in Marine Science*, 4(329), 2017. doi: 10.3389/fmars.2017.00329.

Vanhellemont, Q. and Ruddick, K. G. Turbid wakes associated with offshore wind turbines observed with Landsat 8. *Remote Sensing of Environment*, 145:105–115, 2014. doi: 10.1016/j.rse.2014.01.009.

Vanhellemont, Q. and Ruddick, K. G. Advantages of high quality SWIR bands for ocean colour processing : Examples from Landsat-8. *Remote Sensing of Environment*, 161: 89–106, 2015. doi: 10.1016/j.rse.2015.02.007.

Verpoorter, C., Kutser, T., Seekell, D. A., and Tranvik, L. J. A global inventory of lakes based on high-resolution satellite imagery. *Geophysical Research Letters*, 41(18): 6396–6402, 2014. doi: 10.1002/2014GL060641.

Visser, P. M., Verspagen, J. M. H., Sandrini, G., Stal, L. J., Matthijs, H. C. P., Davis, T. W., Paerl, H. W., and Huisman, J. How rising CO_2 and global warming may stimulate harmful cyanobacterial blooms §. *Harmful Algae*, 54:145–159, 2016. doi: 10.1016/j.hal.2015.12.006.

Wang, G., Lee, Z., Mishra, D. R., and Ma, R. Retrieving absorption coefficients of multiple phytoplankton pigments from hyperspectral remote sensing reflectance measured over cyanobacteria bloom waters. *Limnology and Oceanography: Methods*, 14(7): 432–447, 2016. doi: 10.1002/lom3.10102.
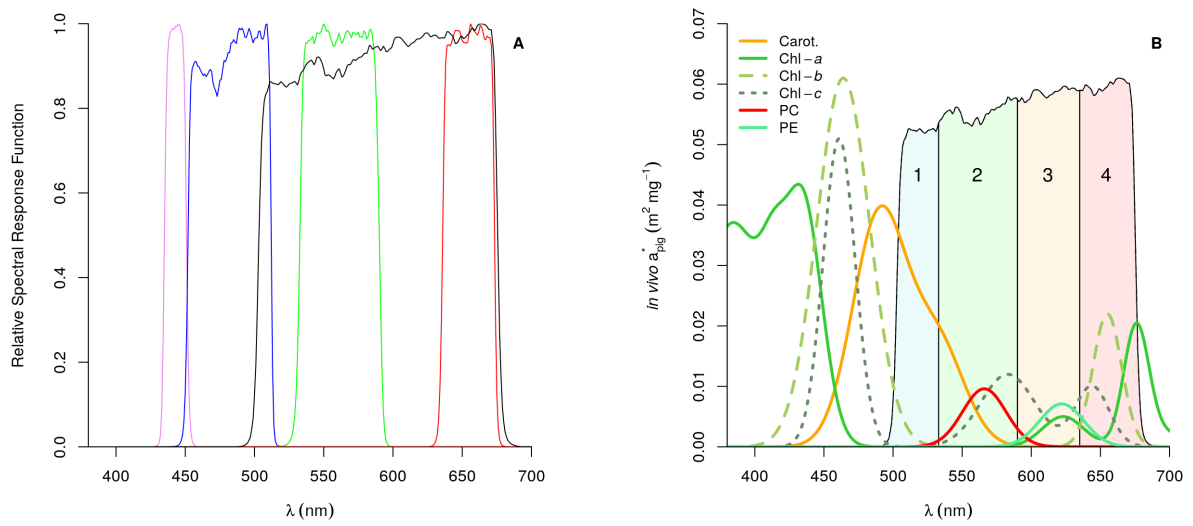
Figure 1: Relative SRFs for OLI sensor. (A) RSRFs for visible range MS bands and Pan; (B) Regions defined in the Pan band superimposed to $^*a_{pig}$ ($\mathrm{m^2\,mg^{-1}}$) (as taken from Hoepffner and Sathyendranath (1993); Wang et al. (2016); and Simis and Kauko (2012)).
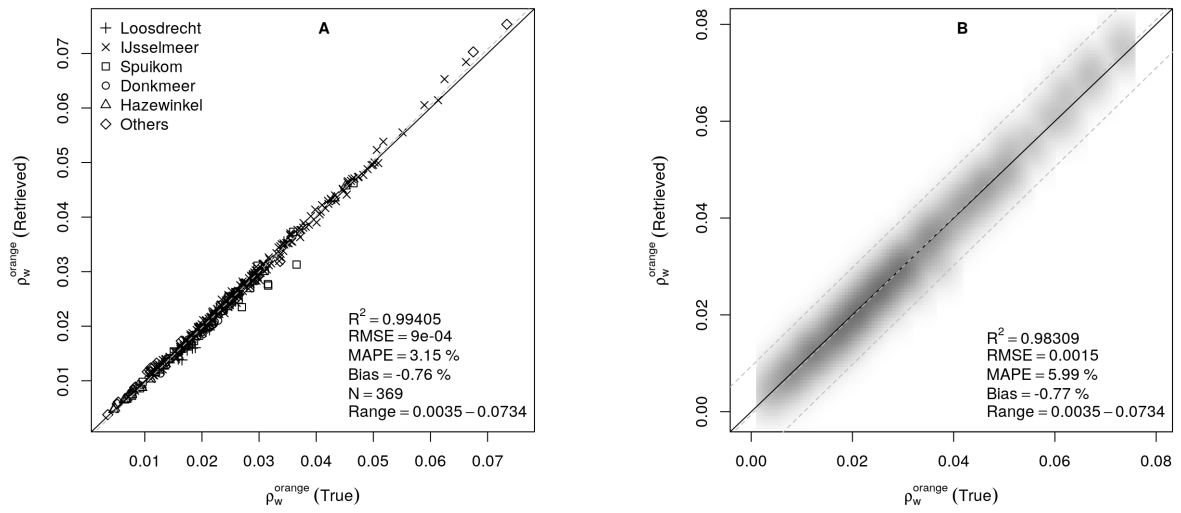
Figure 2: Retrieval of an orange band from OLI Pan and MS bands. (A) Using Eq. 3 in the absence of noise; (B) Using Eq. 3 in the presence of typical random noise for OLI bands. Grey shading in B represents the relative kernel density.
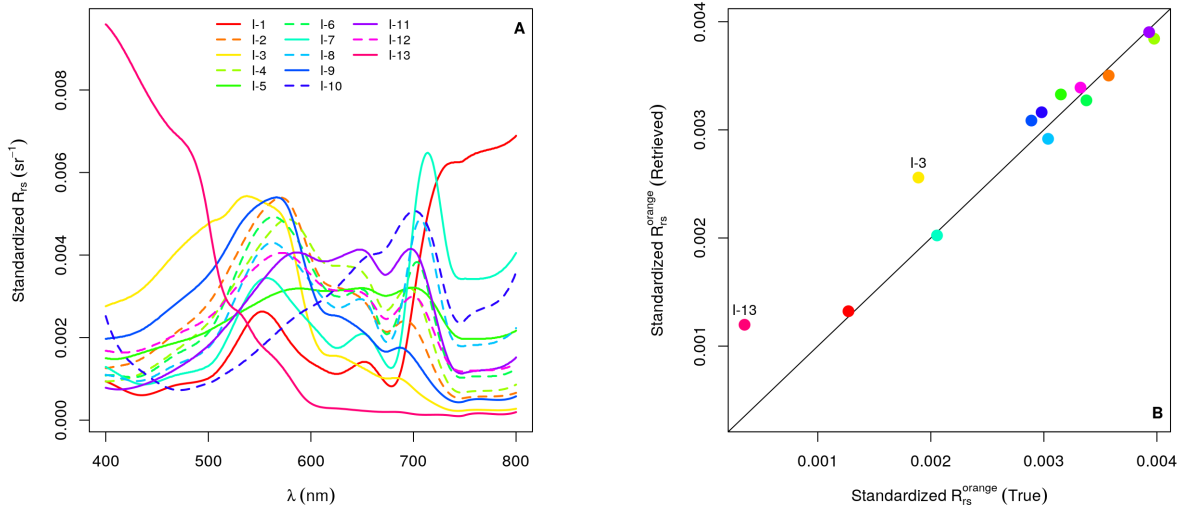
Figure 3: Application of the Eq. 3 to diverse spectral shapes representative of inland waters. (A) The 13 clusters of inland Optical Water Types (Spyrakos et al., 2017); (B) Retrieval results with outliers indicated.
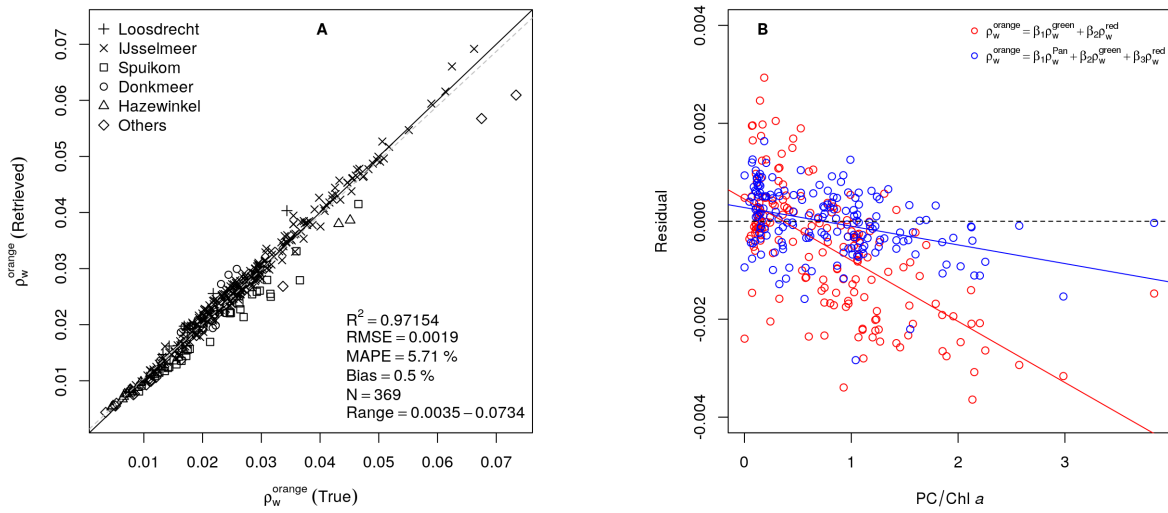
Figure 4: Evaluation of information content of the proposed orange band. (A) regression results for a reduced model excluding the Pan band. (B) Relation between PC to Chl a ratio and model residuals for the full and reduced models. Lines show linear trends in the data. Data for lake IJsselmeer, NL.